Acıbadem Univ. Sağlık Bilim. Derg. 2025; 16 (1)
https://doi.org/10.31067/acusaglik.1569618

ORIGINAL ARTICLE / ARAŞTIRMA YAZISI Bioelectronics, Bioengineering / Biyoelektronik, Biyomühendislik

Clinical Validation of a Custom Wearable Patch for Accurate and Comfortable Vital Sign Monitoring in Pediatric Patients

Beren SEMİZ[1]

[1]Electrical and Electronics Engineering, Koc University, 34450, Istanbul, Turkey

Beren SEMİZ
0000-0002-7544-5974

Correspondence: Beren Semiz
Electrical and Electronics Engineering, Koc University, 34450, Istanbul, Turkey
Phone: +90 533 925 79 91
E-mail: besemiz@ku.edu.tr

Received: 18.10.2024
Accepted: 11.11.2024

ABSTRACT

Background/Purpose: Measuring vital signs in pediatric patients requires special consideration and adaptation due to varying anatomy and wide age range. In addition, children's anxiety, uncooperativeness, and high activity levels further complicate measurements, necessitating devices and algorithms designed to minimize the inaccuracies and discomfort. In this work, the performance of a custom wearable patch mounted on the mid-sternum was validated in uncontrolled settings on a cohort including 84 pediatric patients.

Methods: Three-minute-long electrocardiogram (ECG), seismocardiogram (SCG) and photoplethysmogram (PPG) signals were acquired using the custom patch. First, pre-processing and signal smoothing algorithms were employed to suppress the out-of-band and motion noise. Two different tasks were then studied: (i) Heart rate (HR) and respiration rate were derived from the ECG, PPG and SCG signals individually. During HR derivation from the SCG, a novel Teager-energy-based HR estimation algorithm was proposed. (ii) Clinical relevance of the SCG signals was shown through mapping the SCG characteristics to body mass index (BMI) and blood pressure values.

Results: While the best HR estimation was achieved through the PPG-infrared signal with an absolute error of 2.2±2.1 bpm, the best respiration estimation was achieved with PPG-Red signal with an error of 2.6±2.2 breaths/min. On the other hand, regression models resulted in a minimum of 85% confidence interval, revealing that the SCG characteristics indeed have salient correlation with the BMI and blood pressure values.

Conclusion: Overall, the proposed patch and corresponding algorithms could potentially be leveraged for measuring vital signs from pediatric patients in clinical settings by minimizing the inaccuracies and discomfort encountered.

Keywords: Biomedical signal processing; Hemodynamic parameters; Wearable systems; Electrocardiogram; Seismocardiogram; Photoplethysmogram

ÖZET

Amaç: Pediatrik hastalarda yaşamsal parametrelerin ölçülmesi, değişken anatomi ve geniş yaş aralığı nedeniyle özel dikkat ve adaptasyon gerektirmektedir. Buna ek olarak, çocukların anksiyetesi, yeterince işbirliği yapmaması ve yüksek aktivite seviyeleri ölçümleri daha da karmaşık hale getirmektedir. Bu nedenle hataları ve kullanıcı rahatsızlığını en aza indirmek için tasarlanmış cihazlara ve algoritmalara büyük bir ihtiyaç vardır. Bu çalışmada, 84 pediatrik hastayı içeren bir kohort üzerinde, kontrolsüz ortamlarda, orta sternuma yerleştirilen özel bir giyilebilir yamanın performansı valide edilmiştir.

Yöntem: Yama kullanılarak üç dakikalık elektrokardiyogram (EKG), sismokardiyogram (SCG) ve fotopletismogram (PPG) sinyalleri kaydedilmiştir. İlk olarak, bant dışı ve hareket gürültüsünü bastırmak için ön işleme ve sinyal yumuşatma algoritmaları kullanılmıştır. Ardından iki farklı analiz üzerinde çalışılmıştır: (i) Nabız ve solunum hızı, EKG, PPG ve SCG sinyallerinden ayrı ayrı türetilmiştir. SCG'den nabız türetme sırasında, yeni bir Teager-enerji tabanlı HR tahmin algoritması önerilmiştir. (ii) SCG sinyallerinin klinikte kullanılabilirliği, SCG özelliklerinin vücut kitle indeksi (BMI) ve kan basıncı değerleriyle eşleştirilmesiyle değerlendirilmiştir.

Bulgular: En iyi nabız tahmini 2.2±2.1 bpm mutlak hata ile PPG-kızılötesi sinyali ile elde edilirken, en iyi solunum tahmini 2.6±2.2 nefes/dak hata ile PPG-Kırmızı sinyalinden elde edilmiştir. Öte yandan, regresyon modelleri minimum %85 güven aralığıyla sonuçlanmış ve SCG özelliklerinin BMI ve kan basıncı değerleri ile belirgin bir korelasyona sahip olduğunu ortaya koymuştur.

Sonuç: Önerilen yama ve ilgili algoritmalar, klinik ortamlarda karşılaşılan yanlışlıkları ve rahatsızlıkları en aza indirerek pediatrik hastaların yaşamsal belirtilerini ölçmek için potansiyel olarak kullanılabilir.

Anahtar Kelimeler: Biyomedikal sinyal işleme; Hemodinamik parametreler; Giyilebilir sistemler; Elektrokardiyogram; Sismokardiyogram; Fotopletismogram

Each year, pediatric clinics around the world admit millions of young patients, encompassing a diverse spectrum of medical needs and conditions. Based on the National Health Interview Survey reported by the Centers for Disease Control and Prevention, 95.0% of the children had a visit with a health care professional in 2023 (1). The clinical assessments during these visits often involve assessing vital signs like heart rate, respiration, blood pressure, and temperature, along with heart, lung, and vascular evaluations. Such assessments support accurate diagnosis, monitor treatment, and help ensure the well-being of pediatric patients globally (2-4).

Measuring vital signs in pediatric patients presents unique challenges, as devices designed for adults may not be suitable for children's smaller size, wider age range (from newborns to adolescents) and anatomical features (5). Indeed, pediatric devices tend to be less advanced and available compared to adult devices, often trailing by up to around 10 years in technological development (6). Second, children may be anxious or uncooperative during vital sign assessments, introducing motion artifacts and affecting the reliability of readings (2). It has been found that 91% of children reported fear related to medical procedures, with 28% associating clinical exams with pain and 29% being scared of nursing activities (7). Thus, devices and algorithms for pediatric population should be designed in a way that the discomfort and inaccuracies are minimized.

Physiological signals like the electrocardiogram (ECG), seismocardiogram (SCG) and photoplethsmogram (PPG) are essential in wearables, as they directly originate from the underlying physiology. The ECG assesses the heart's electrical activity, while the SCG detects vibrations originating from heart contractions, with peaks and valleys reflecting cardiac events like aortic opening (AO), mitral closing (MC), etc. (8). Recent studies have utilized the SCG signal for various applications, ranging from estimating hemodynamic parameters to assessing valvular heart diseases (9-14). Finally, the PPG detects changes in light absorption caused by variations in arterial blood volume during the cardiac cycle. Analyzing PPG provides insights into blood oxygen levels, blood pressure, and vascular resistance (15-18). Thus, integrating physiological signals into wearable devices is a major advancement in healthcare, enhancing preventive care and supporting better health outcomes worldwide (19).

In this work, *for the first time*, the performance of a custom wearable patch was investigated in *uncontrolled settings* on a cohort including 84 pediatric patients visiting Koc University Hospital. The study involved the continuous acquisition of 3-minute-long ECG, tri-axial SCG and PPG (red and infra-red) signals. After pre-processing, heart rate (HR) and respiration rate were calculated using novel signal processing pipelines. Clinical relevance was assessed by performing regression analyses that mapped SCG features to body mass index (BMI) and blood pressure values.

Material and Methods

In this work, we adapted our previously developed custom wearable patch and, *for the first time*, validated its clinical performance in uncontrolled settings on a cohort including 84 pediatric patients visiting Koc University Hospital from March to April 2024. Figure 1 shows the patch's hardware layers and attachment locations.

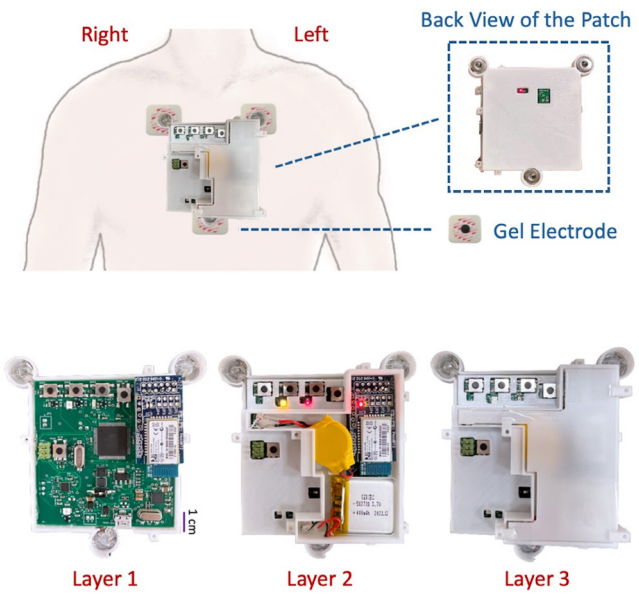

Figure 1: The wearable patch used in data collection

2.1 Custom Hardware

The SCG and PPG were acquired using an ADXL355 accelerometer (at 500 Hz) and a MAX30102 sensor (at 200 Hz), respectively. The ECG was recorded with an AD8232 analog front-end integrated circuit, through three gel electrodes to form Einthoven's triangle. Skin temperature was measured using an LMT70A sensor. The ECG and temperature were sampled at 500 Hz and 25 Hz with 10-bit resolution. As the microcontroller, ATMEGA2560 was used. Data was written to a file on a microSD card, with file naming controlled by the DS3231 real-time clock. The system ran on a 400 mAh Lithium-Polymer battery, charged via an LTC4062 charger, with hardware interrupts for optimized power management. The hardware and firmware specifications are detailed in (20).

2.2 Data Collection Protocol

The study was conducted under a protocol approved by the Koc University Institutional Review Board (2023.408.IRB2.089) and all parents/guardians have provided their written consent. 84 children were participated in the study. Before data collection, the baseline values for the body temperature, oxygen saturation (SpO2), heart rate (HR), and systolic and diastolic blood pressures (SBP and DBP) were measured. The demographics and baseline hemodynamic parameters are presented in Table I.

Table 1. Subject demographics (mean ± std)

Age (years) 9.1 ± 4.3	**Weight** (kg) 33.9 ± 18.3	**Height** (cm) 131.4 ± 26.3
BMI (kg/m^2) 18.1 ± 3.9	**Gender** 50.0 % Female 50.0 % Male	**Chronic Disease** 26.6 % Yes 71.4 % No
Heart Rate (bpm) 103.8 ± 22.7	**Temperature** (Celsius) 37.0 ± 0.6	**SpO_2** (%) 96.7 ± 3.6
Respiration Rate (breaths/min) 23.4 ± 4.1	**Systolic BP** (mmHg) 109.4 ± 14.0	**Diastolic BP** (mmHg) 74.4 ± 12.5

Data collection took place in a room in pediatric clinic without specific environmental restrictions, as factors like sound, humidity, and lighting did not impact the signals. The patch was placed on the mid-sternum using three gel electrodes, and to minimize motion artifacts, subjects sat still in a relaxed state for three minutes. The ECG, SCG and PPG signals were acquired continuously with sampling rates of 500, 500 and 200 Hz, respectively. The start and end moments of the three-minute period were determined by gently tapping on the patch, generating two distinct peaks on the SCG signals. The challenges regarding the clinical implementation are covered in the Discussion section.

Analyses were conducted on the entire dataset, followed by sub-group analyses based on:

- *Age groups:* Pre-school ($y < 6$, $n = 20$, 4.2 ± 1.3), Elementary-school ($6 \leq y < 11$, $n = 37$, 8.0 ± 1.2), Middle-school ($11 \leq y < 14$, $n = 8$, 11.3 ± 0.7), and High-school ($14 \leq y \leq 18$, $n = 19$, 15.7 ± 1.3).
- *Gender:* 42 subjects each for female and male groups.
- *Chronic disease status:* 24 subjects with chronic disease and 60 without

2.3 Signal Pre-Processing

After data collection, signal processing pipelines for estimating hemodynamic parameters were developed (Figure 2(a)). The signals were filtered with Kaiser window FIR bandpass filters to reduce noise while maintaining signal integrity. To calculate the heart rate, cut-off frequencies of 1-15 Hz for PPG, 0.5-40 Hz for ECG, and 1-40 Hz for SCG were used as per the literature (21, 22). Figure 3 shows representative four-second segments of filtered ECG, SCG, and PPG signals from one subject.

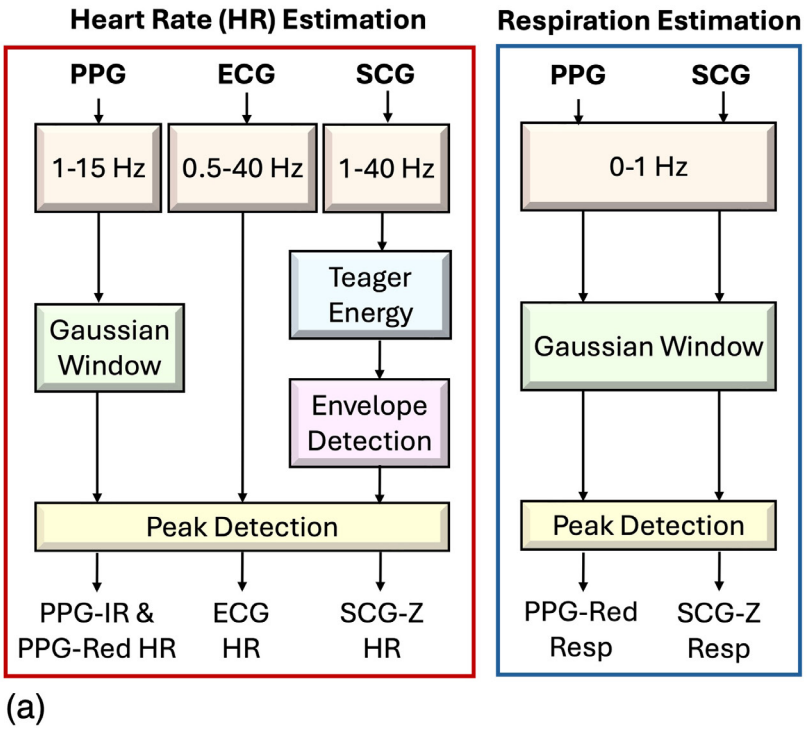

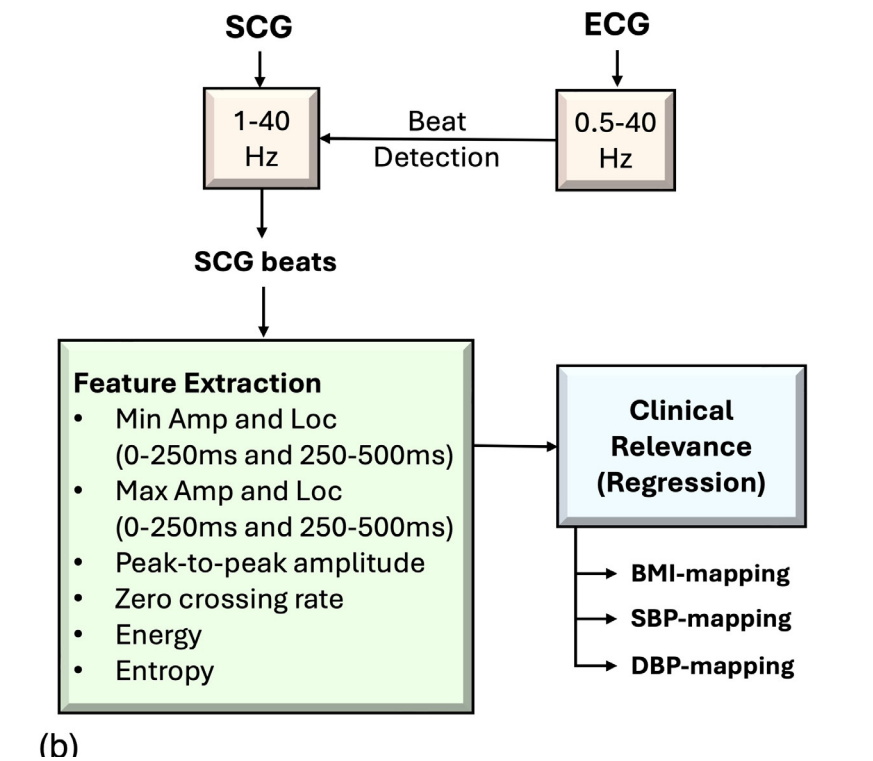

Figure 2: (a) Pre-processing and signal processing pipelines for the estimation of hemodynamic parameters, **(b)** Pre-processing and signal processing pipelines for the clinical relevance assessment tasks, *Min: minimum, Max: maximum, Amp: amplitude, Loc: location, BMI: body mass index, SBP: systolic blood pressure, DBP: diastolic blood pressure*

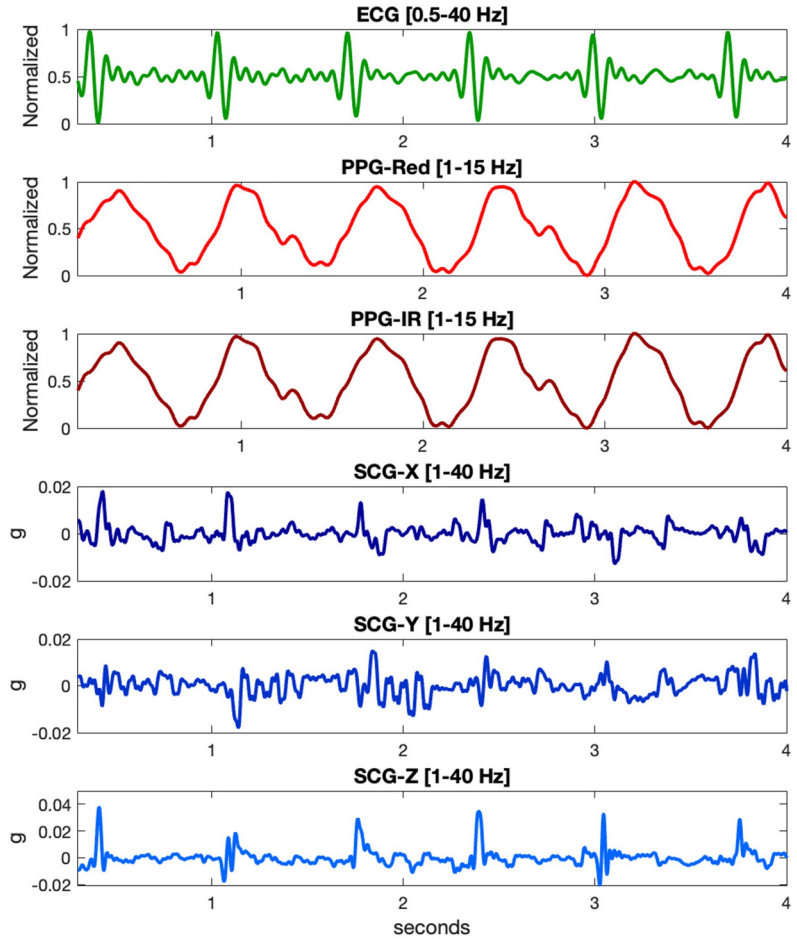

Figure 3: Four-second long segments of the collected signals

On the other hand, the frequencies below 1 Hz represent the respiration information corresponding to the respiration-induced chest movements (23). Hence, while extracting respiratory information from the SCG and PPG signals, the original raw signals were filtered using an upper cut-off frequency as 1 Hz. The PPG and SCG signals were then Gaussian filtered to remove the motion artifacts for ease of peak detection. The Gaussian window was applied to the signal, averaging the points to smooth high-frequency noise while retaining signal characteristics. The Gaussian window and width factor (alpha) values were determined heuristically to ensure that the signals were not over-smoothed (losing fiducial points) or under-smoothed (having redundant fluctuations). For the PPG and SCG signals, the window size and width factor pairs were selected as (25, 2.3) and (250, 2.3), respectively, in alignment with the corresponding sampling rates.

2.4 Estimation Hemodynamic Parameters

2.4.1 Estimation of Heart Rate from ECG and PPG Signals

To compute the HR values from the collected signals, the following steps were implemented:

1) As the reference values, the baseline HR measurements acquired prior to data collection were used.

2) For the ECG-based computation, the filtered signal (0.5-40 Hz) was first normalized. Then, the R-peaks were detected with a simple peak detection algorithm (minimum peak height: 0.6, minimum peak distance: 0.33 of the sampling rate). The consecutive R-peak intervals formed an RR difference vector, which was used to calculate heart rate (HR) in beats per minute (bpm) using Equation 1.

3) For the PPG-based computation, the time intervals between the consecutive peaks on the filtered (1-15 Hz) and Gaussian-windowed red and infrared PPG signals were computed, and stored as a PP difference vector, similar to the ECG case.

4) Equations 2 and 3 were used to calculate the mean absolute error (MAE) and percentage error, where 'actual' refers to the reference HR values and 'calculated' refers to the HR values derived from the ECG, PPG-red, and PPG-infrared signals *(Fs: sampling rate, std: standard deviation)*.

$$HR = \frac{60*Fs}{mean(RR)} \quad (1)$$

$$MAE = |actual - calculated| \quad (2)$$

$$\%\ error = \frac{|actual-calculated|}{actual} * 100 \quad (3)$$

2.4.2 Teager-Operator-based Heart Rate Estimation from SCG Signals

The Teager energy operator, derived from the energy of an oscillator, detects instantaneous changes in signals, such as amplitude variations, frequency shifts, or discontinuities (24). In our previous work, the Teager operator was leveraged to locate the clicks in the joint sound signals acquired from the children with juvenile idiopathic arthritis (25). When an SCG signal is considered, detecting the aortic opening (AO) points using a simple peak detection algorithm can be challenging as (i) there are additional neighboring peaks representing mitral closing (MC) and aortic closing (AC) moments, and (ii) there are added noise due to motion artifacts and signal variability, which make AO points more subtle. Hence, we hypothesized that the Teager energy operator could accurately locate AO points, even when simple peak detection algorithms fail.

For any discrete-time signal , the Teager energy () at time is calculated using the three consecutive samples of the signal as in Equation 4.

$$\Psi_{TE}[n] = x[n]^2 - x[n+1]x[n-1] \quad (4)$$

In this work, the Teager energy of the filtered SCG-Z signal (1-40 Hz) was calculated (Equation 4). The upper envelope of the Teager operator was then generated to emphasize significant peaks representing the AO points (26). The time intervals between consecutive spikes were computed, and their mean value was used to calculate the HR (Equation 1). Error calculations were done using Equations 2 and 3.

2.4.3 Estimation of Respiration

To calculate the respiration rate, two different approaches (SCG-Z-based and PPG-Red-based) were used. PPG-Red was chosen over PPG-IR, as it is less prone to motion artifacts due to relatively lower wavelength. As previously explained, both signals were filtered between 0-1 Hz and smoothed with a Gaussian window. Peak-to-peak intervals were then calculated, with the peak-valley transitions corresponding to exhalation-inhalation cycles, where each peak-to-peak duration represents a full respiration cycle. The resulting peak-to-peak vector was then used in an equation similar to Equation 1, and respiration rate in breaths/min was calculated. The errors were again calculated using Equations 2 and 3.

2.4.4 Investigating the Clinical Relevance of SCG

The clinical relevance of SCG signal characteristics was assessed by correlating them with physiological parameters (Figure 2(b)). The R-peaks from the ECG (0.5-40 Hz) were leveraged to divide the SCG-Z (1-40 Hz) into individual beats, each truncated to the minimum R-R interval length. A total of 13,603 SCG-Z beats from 84 subjects were analyzed, extracting 12 temporal features per beat (27): the minimum and maximum amplitudes and corresponding locations within the systolic (0-250ms) and diastolic (250-500ms) portions, peak-to-peak amplitude, energy, entropy and zero-crossing rate. Three XGBoost regression models were trained to map the SCG characteristics to body mass index (BMI), sytolic blood pressure (SBP), and diastolic blood pressure (DBP), with performances validated using 5-fold cross-validation and assessed by mean absolute percentage error (MAPE).

Results

3.4.1 Estimation of Heart Rate from ECG and PPG Signals

The absolute and percentage errors for ECG and PPG-based calculations were presented in Table 2, and the boxplots for absolute errors are shown in Figure 4. While the ECG-derived resulted in an absolute and percentage errors of 4.9 ± 6.7 bpm and 4.7 ± 6.8 %, respectively; these values were 2.5 ± 2.4 bpm and 2.3 ± 1.9 % for the PPG-Red, and 2.2 ± 2.1 bpm and 2.1 ± 1.9 % for the PPG-IR.

3.4.2 Teager-Operator-based Heart Rate Estimation from SCG Signals

Figure 5(a) shows a 10-second SCG signal and its Teager energy plot. While some SCG segments (green box) were clean enough for accurate peak detection, others (yellow box) contained motion noise. Direct peak detection in the noisy regions would thus be unreliable, but the Teager operator successfully identified the AO peaks in these areas, allowing for accurate HR computation. Our algorithm yielded absolute and percentage errors of 4.6 ± 5.4 bpm and 4.4 ± 6.0 %, respectively (Table 2). This result was indeed comparable to the one obtained from ECG and suggests a confidence interval of at least 95%. The corresponding boxplots for absolute errors are shown in Figure 4.

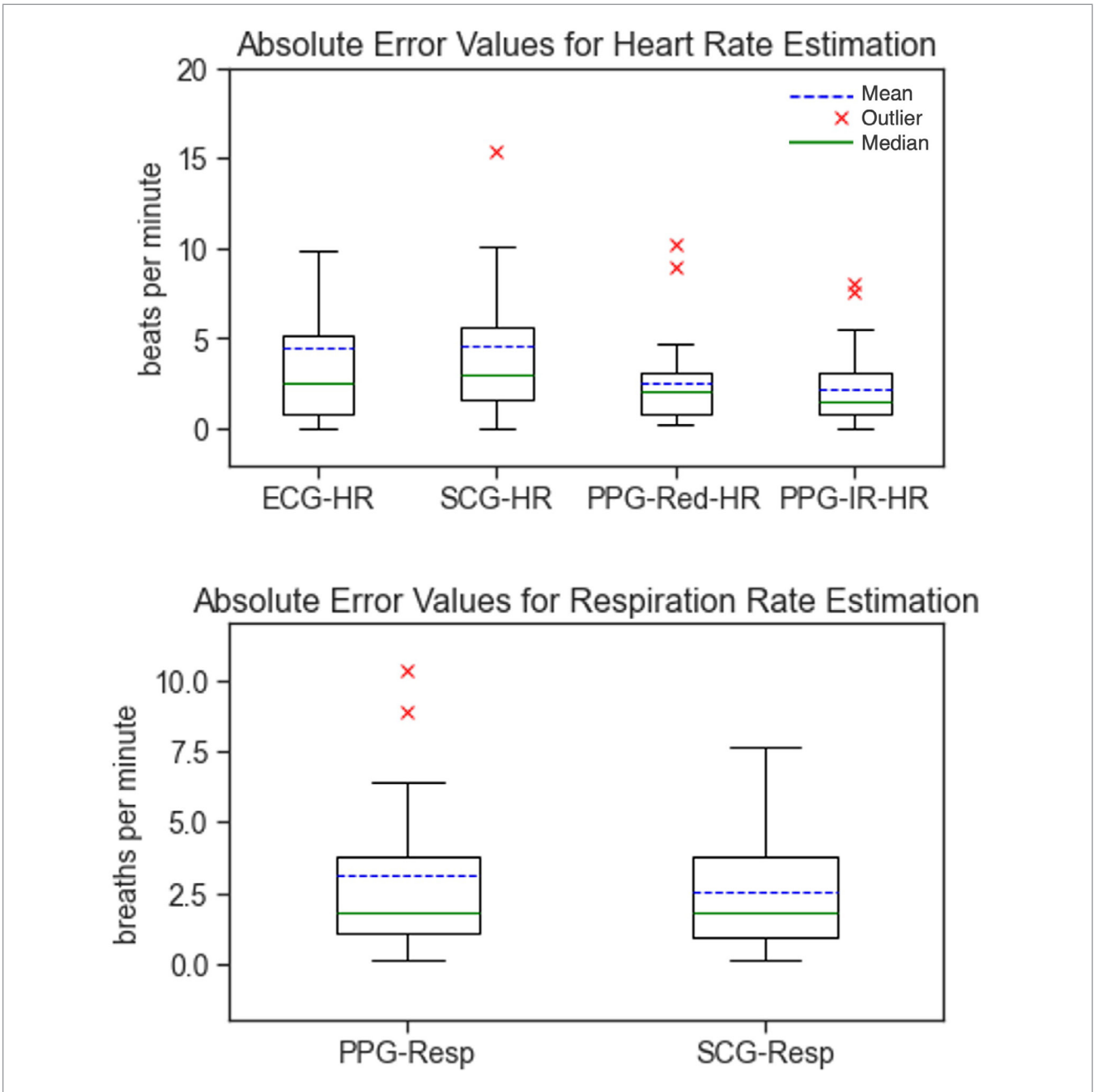

Figure 4: Box plots representing the absolute error values for heart rate and respiration rate estimation tasks.

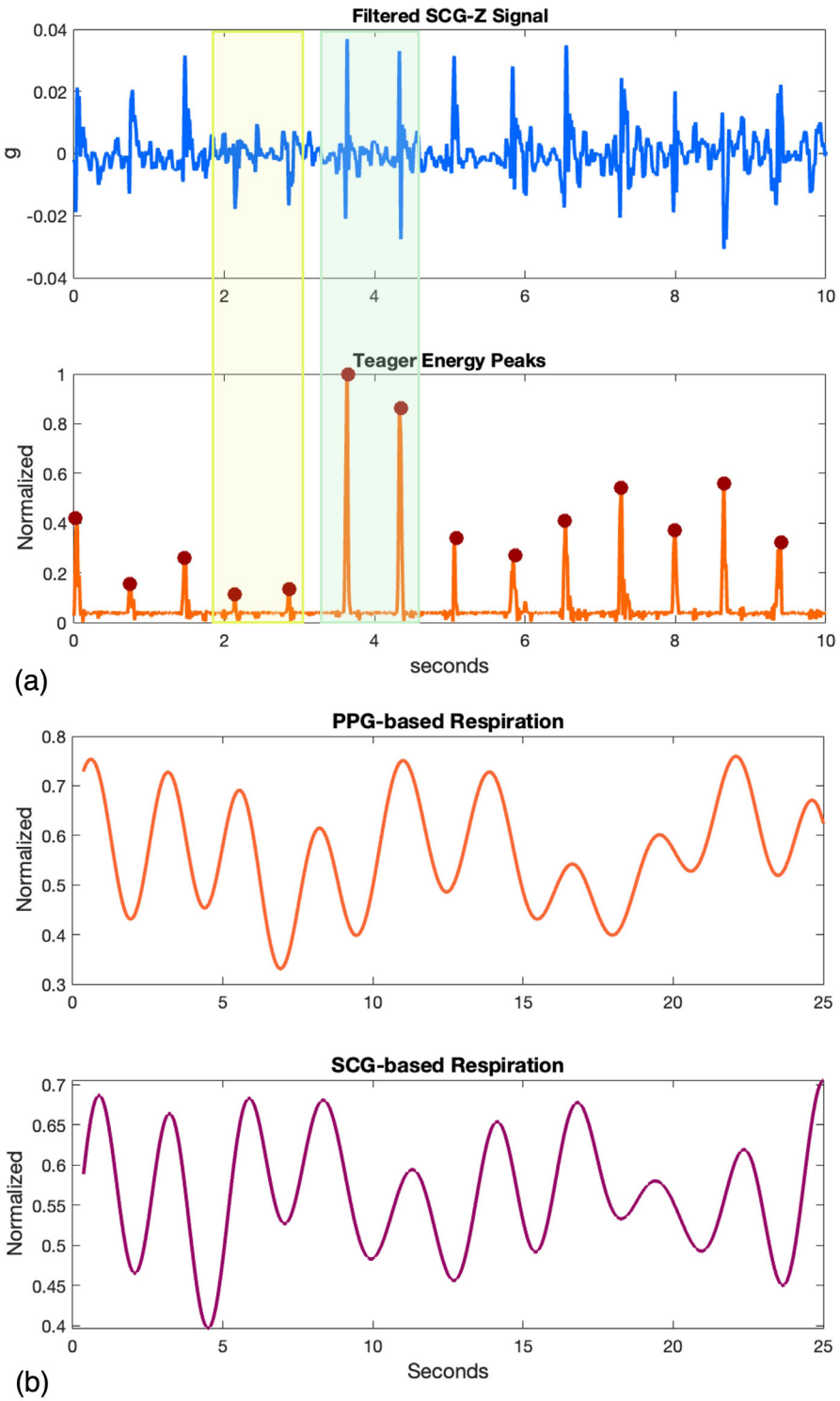

Figure 5: (a) Teager energy operator of a 10-second long SCG segment and detected beats, **(b)** Five-second long respiration signals derived from SCG and PPG signals

3.4.3 Estimation of Respiration

To derive the respiration information, an SCG-Z-based and PPG-Red-based derivation pipelines were used and compared. Sample five-second-long segments from the resulting signals are presented in Figure 5(b). As seen, the oscillation patterns are the same with a slight variance in the amplitude values. This was expected as the sensors are located in different regions on the patch. The estimated respiration rates are presented in Table 2. While the respiration rate estimated from PPG-Red resulted in an absolute error and percentage error of 2.6 ± 2.2 breaths/min and 11.5 ± 10.3 %; these results were 3.1 ± 3.2 breaths/min and 12.9 ± 11.1 % for the SCG-Z-based derivation.

3.4.4 Investigating the Clinical Relevance of SCG

For the BMI-, SBP- and DBP-mapping tasks, the train and test MAPE pairs were (11.3%, 14.4%), (9.7%, 11.5%) and (9.2%, 11.1%), respectively (Table 2). Overall, all models resulted in a minimum of 85% confidence interval, revealing that the SCG characteristics indeed have salient correlation with the BMI, SBP and DBP values.

Table 2. Estimated Cardiovascular Parameters (mean ± std) and results for the regression tasks

	Absolute Error	**Percentage Error**
ECG HR	4.9 ± 6.7 bpm	4.7 ± 6.8 %
PPG-Red HR	2.5 ± 2.4 bpm	2.3 ± 1.9 %
PPG-IR HR	2.2 ± 2.1 bpm	2.1 ± 1.9 %
SCG HR	4.6 ± 5.4 bpm	4.4 ± 6.0 %
PPG-Red Respiration	2.6 ± 2.2 breaths/min	11.5 ± 10.3 %
SCG-Z Respiration	3.1 ± 3.2 breaths/min	12.9 ± 11.1 %
Clinical Relevance (Regression Task)		
	5-fold Train MAPE	**5-Fold Test MAPE**
BMI-mapping	11.3% error (88.7% confidence)	14.4% error (85.6% confidence)
SBP-mapping	9.7% error (90.3% confidence)	11.5% error (88.5% confidence)
DBP-mapping	9.2% error (90.8% confidence)	11.1% error (88.9% confidence)

Sub-group results revealed a general decrease in error rates for both heart rate and respiration rate measurements as age increases (Table 3). When the effect of gender was investigated, male patients showed relatively lower errors in heart rate estimation and regression tasks, while females exhibited lower errors in respiration rate analysis (Table 4). On the other hand, for all analyses, patients with chronic disease resulted in lower errors compared to the ones not having.

Table 3. Sub-group Analysis for Different Age Groups (mean ± std)

		Heart Rate			
		ECG	**SCG**	**PPG-Red**	**PPG-IR**
Pre-School (y < 6)	Abs err	8.1 ± 10.1 bpm	7.3 ± 8.4 bpm	5.1 ± 4.3 bpm	3.3 ± 3.4 bpm
	% error	7.7 ± 11.0 %	6.6 ± 9.1 %	3.9 ± 3.1 %	2.8 ± 2.7 %
Elem-School (6 ≤ y < 11)	Abs err	4.6 ± 6.2 bpm	4.0 ± 4.5 bpm	**1.7 ± 1.3 bpm**	**1.4 ± 1.0 bpm**
	% error	4.2 ± 5.6 %	3.8 ± 4.2 %	1.6 ± 1.1 %	1.3 ± 0.9 %
Mid-School (11 ≤ y < 14)	Abs err	3.6 ± 2.9 bpm	4.7 ± 3.3 bpm	3.2 ± 1.4 bpm	5.9 ± 2.9 bpm
	% error	3.5 ± 2.8 %	4.3 ± 3.2 %	3.0 ± 1.9 %	5.5 ± 3.4 %
High-School (14 ≤ y ≤ 18)	Abs err	**2.9 ± 3.1 bpm**	**3.3 ± 4.3 bpm**	**2.1 ± 1.3 bpm**	**2.3 ± 1.2 bpm**
	% error	3.3 ± 4.3 %	3.9 ± 6.8 %	2.3 ± 1.7 %	2.5 ± 1.6 %

		Respiration Rate	
		SCG	**PPG**
Pre-School (y < 6)	Abs err	5.0 ± 3.0 breath/min	7.3 ± 4.8 breath/min
	% error	19.3 ± 11.5 %	26.4 ± 14.8 %
Elem-School (6 ≤ y < 11)	Abs err	2.1 ± 1.7 breath/min	2.2 ± 1.6 breath/min
	% error	10.1 ± 10.2 %	10.1 ± 7.4 %
Mid-School (11 ≤ y < 14)	Abs err	3.4 ± 2.7 breath/min	2.7 ± 1.4 breath/min
	% error	17.4 ± 12.8 %	14.1 ± 6.4 %
High-School (14 ≤ y ≤ 18)	Abs err	**1.3 ± 0.7 breath/min**	**2.0 ± 2.6 breath/min**
	% error	5.7 ± 3.2 %	8.4 ± 10.8 %

		Clinical Relevance (Regression Task) – 5 fold		
		SBP	**DBP**	**BMI**
Pre-School (y < 6)	Train Mape	4.8 ± 0.6 %	9.2 ± 1.2 %	4.9 ± 0.1 %
	Test Mape	6.5 ± 0.5 %	11.9 ± 0.8 %	6.8 ± 0.5 %
Elem-School (6 ≤ y < 11)	Train Mape	6.2 ± 0.5 %	7.9 ± 0.1 %	9.1 ± 0.1 %
	Test Mape	7.9 ± 0.3 %	10.4 ± 0.5 %	12.0 ± 0.5 %
Mid-School (11 ≤ y < 14)	Train Mape	4.6 ± 0.4 %	3.9 ± 0.1 %	4.4 ± 0.1 %
	Test Mape	5.4 ± 0.2 %	**5.5 ± 0.6 %**	**6.1 ± 0.3 %**
High-School (14 ≤ y ≤ 18)	Train Mape	3.9 ± 0.1%	4.9 ± 0.1 %	8.4 ± 0.1 %
	Test Mape	**5.3 ± 0.3 %**	6.4 ± 0.2 %	11.3 ± 0.5 %

Table 4. Sub-group Analysis for Different Genders and Chronic Disease Conditions (mean ± std)

GENDER-BASED GROUPING		Heart Rate			
		ECG	SCG	PPG-Red	PPG-IR
Female	Abs err	5.2 ± 6.7 bpm	5.2 ± 5.4 bpm	3.0 ± 2.9 bpm	2.3± 2.0 bpm
	% error	5.4 ± 7.7 %	5.4 ± 6.9 %	2.6 ± 2.1 %	2.3 ± 2.1 %
Male	Abs err	**4.5 ± 6.6 bpm**	**3.9 ± 5.5 bpm**	**1.9 ± 1.4 bpm**	**2.2 ± 2.1 bpm**
	% error	4.0 ± 5.7 %	3.3 ± 4.7 %	1.9 ± 1.5 %	1.9 ± 1.6 %

DISEASE-BASED GROUPING		Heart Rate			
		ECG	SCG	PPG-Red	PPG-IR
Chronic Disease	Abs err	**2.7 ± 2.6 bpm**	**3.2 ± 3.7 bpm**	**1.3 ± 1.2 bpm**	**1.7 ± 1.2 bpm**
	% error	2.8 ± 3.6 %	3.6 ± 5.7 %	1.3 ± 1.3 %	1.6 ± 1.1 %
NO Chronic Disease	Abs err	5.9 ± 7.6 bpm	5.2 ± 6.0 bpm	2.8 ± 2.5 bpm	2.4 ± 2.2 bpm
	% error	5.6 ± 7.7 %	4.8 ± 6.1%	2.5 ± 1.9 %	2.2 ± 2.1 %

GENDER-BASED GROUPING		Respiration Rate	
		SCG	PPG
Female	Abs err	**2.5 ± 2.4 breath/min**	**2.9 ± 3.1 breath/min**
	% error	11.6 ± 12.1 %	12.2 ± 11.1 %
Male	Abs err	2.6 ± 2.1 breath/min	3.4 ± 3.3 breath/min
	% error	11.4 ± 8.3 %	13.9 ± 11.0 %

DISEASE-BASED GROUPING		Respiration Rate	
		SCG	PPG
Chronic Disease	Abs err	**1.9 ± 2.3 breath/min**	**0.2 ± 0.1 breath/min**
	% error	10.7 ± 15.1 %	4.3 ± 4.5 %
NO Chronic Disease	Abs err	2.7 ± 2.2 breath/min	3.7 ± 3.3 breath/min
	% error	11.7 ± 9.0 %	15.3 ± 11.2 %

GENDER-BASED GROUPING		Clinical Relevance (Regression Task) – 5 fold		
		SBP	DBP	BMI
Female	Train Mape	9.5 ± 0.4 %	8.4 ± 0.1 %	10.4 ± 0.1 %
	Test Mape	11.2 ± 0.3 %	11.1 ± 0.3 %	13.9 ± 0.5 %
Male	Train Mape	7.5 ± 0.7 %	6.1 ± 0.1 %	9.9 ± 0.1 %
	Test Mape	**9.4 ± 0.2 %**	**8.3 ± 0.2 %**	**12.9 ± 0.3 %**

DISEASE-BASED GROUPING		Clinical Relevance (Regression Task) – 5 fold		
		SBP	DBP	BMI
Chronic Disease	Train Mape	5.9 ± 0.1 %	7.1 ± 0.1 %	10.5 ± 0.1%
	Test Mape	**8.1 ± 0.3 %**	**9.5 ± 0.5 %**	**12.4 ± 5.7 %**
NO Chronic Disease	Train Mape	10.2 ± 0.2 %	9.1 ± 0.1 %	10.5 ± 0.1%
	Test Mape	12.1 ± 1.7 %	11.1 ± 0.4 %	13.6 ± 0.4 %

Discussion

PPG-derived HR trials resulted in lower errors than ECG-derived HR, contrary to the expectations. This may be due to two factors: (i) The ECG signal quality was compromised by motion and contact loss between the skin and electrodes, as children often get nervous and sweat in clinical settings. (ii) PPG signals were smoothed with a Gaussian window, reducing oscillations and noise while preserving key peaks, making peak detection more accurate.

On the other hand, deriving HR from SCG has always been challenging due to the noise from movement and complex waveform. Additionally, it contains multiple neighbouring peaks corresponding to various cardiac phases, making AO point identification difficult. Our proposed approach's superior performance has been compared with the common methods in the literature as well (Table 5). These methods were including direct peak detection, template matching with correlation computation (28) and wavelet decomposition (29). Among these, the closest results were obtained when wavelet decomposition was used, whereas template matching and direct peak detection suffered from inaccuracies due to motion-related variation in the SCG morphology. Hence, given SCG's common use in wearable systems, this Teager-based method can enhance vital parameter monitoring while reducing computational and hardware demands.

Table 5. Comparison with the literature for the SCG-based HR methods

METHOD		Absolute Error	% Error
Direct Peak Detection	Without envelope	6.4 ± 6.2 bpm	6.1 ± 6.2 %
	With envelope	5.9 ± 7.1 bpm	5.8 ± 7.4 %
Template Matching with Correlation Computation (28)		16.1 ± 14.9 bpm	17.3 ± 19.7 %
Wavelet Decomposition (29)	Without envelope	5.6 ± 7.2 bpm	5.7 ± 7.7 %
	With envelope	5.5 ± 7.1 bpm	5.5 ± 7.5 %
Teager Energy Operator	Without envelope	5.8 ± 7.4 bpm	5.6 ± 7.9 %
	With envelope	**4.6 ± 5.4 bpm**	**4.4 ± 6.0 %**

In respiration derivation, both SCG- and PPG-based methods showed similar performance, with the PPG-Red method slightly outperforming SCG-Z. The 3-breath error could be attributed to signal quality, but another factor might be the reliability of the reference measurement. The reference respiration rate was determined using manual breath counting rather than a digital tool, which could have introduced inaccuracies that were reflected in the algorithm's output.

The clinical relevance of SCG was also observable in the BMI and blood pressure mapping models.

The transmission of vibrations from the heart to the accelerometer is influenced by various tissues such as bone, muscle, fat, and skin, whose composition and thickness vary across individuals (30). These anatomical differences impact SCG characteristics, which were observed in our BMI estimation results in parallel. Similarly, the SBP and DBP estimation tasks resulted in satisfactory performance. As previously explained, the peaks and valleys of the SCG signal represent cardiac valve movements, similar to the blood pressure waveform where the valleys mark aortic valve opening (diastolic pressure) and the dicrotic notch corresponds to aortic valve closure. Literature demonstrates that time differences between fiducial points in the ECG, SCG, and PPG signals can be used in pulse arrival time (PAT) and pulse transit time (PTT)-based blood pressure estimation (31-33). However, these approaches require two different signals to derive the blood pressure values. On the other hand, in our work, we showed that the SCG signal features could directly be mapped to blood pressure values, without requiring any additional signals. This might potentially contribute to alleviate the computational or hardware-related needs.

When sub-groups results were investigated, PPG methods showed lower errors across all age groups in all tasks. For

SBP, DBP, and BMI analyses, older children (middle and high school) exhibited lower error rates, suggesting more stable measurements. When gender results were investigated, anatomical differences, particularly the higher fat-to-muscle ratio in females, affect patch placement and signal quality in HR estimation, though this anatomical variation may improve respiration rate accuracy by enhancing chest expansion detection. Lastly, patients with chronic diseases exhibit significantly lower errors across all measurement methods compared to those without chronic conditions, suggesting more coherent signals and improved model performance, likely due to more consistent physiological responses.

Limitations and Challenges

The study was limited by the relatively small sample size and imbalance across age sub-groups, which may affect the generalizability across and comparability within specific demographic categories. Future work should focus on validating the system with larger, more diverse datasets, including subjects with varying clinical conditions and demographics. Additionally, incorporating longitudinal data could offer insights into the system's long-term effectiveness across different pediatric populations.

A key challenge for clinical implementation is ensuring data accuracy and reliability. Factors such as device placement, sensor quality, and patient movement can lead to inconsistent readings. Children's nervousness can result in sweating and excessive motion, causing electrode contact loss, affecting data quality and creating intra- and inter-subject variability. Additionally, some children and parents expressed concerns about the wearable patch's unfamiliarity and potential long-term effects, which may hinder acceptance and implementation. Addressing these concerns requires targeted education and reassurance to improve user confidence and adherence.

Conclusion

In this study, the performance of our custom wearable patch was evaluated in uncontrolled settings with 84 pediatric patients at Koc University Hospital. The first part involved computing hemodynamic parameters such as heart rate and respiration rate from ECG, PPG, and SCG signals. The second part assessed the clinical relevance by using regression analyses to correlate SCG characteristics with BMI, DBP and SBP. Future work will focus on refining the algorithms and validating the patch's effectiveness in disease monitoring and treatment.

Declarations

Funding

This work was supported by the Scientific and Technological Research Council of Turkey (Grant Number: 121E133).

Conflicts of interest/Competing interest

The authors do not have any conflict of interest or competing interest to disclose.

Ethics Approval

The study was conducted under a protocol approved by the Koc University Institutional Review Board (2023.408.IRB2.089) and all parents/guardians have provided their written consent.

Availability of data and material

The data is not publicly available due to ethical reasons.

Authors contributions

B.S.: Conceptualization, Methodology, Software, Validation, Formal analysis, Investigation, Writing – original draft, Writing – review and editing, Visualization, Funding acquisition

Acknowledgements

This work was supported by the Scientific and Technological Research Council of Turkey (Grant Number: 121E133).

The corresponding author would like to thank Dr. Remziye Semerci, Hatice Seyrek and Ferzin Sinem Opak for their support during data collection, and Yusuf Ziya Hayirlioglu for his support during the hardware design.

References

1. Cdc. National Center for Health Statistics. Percentage of having a doctor visit for any reason in the past 12 months for children under age 18 years, United States, 2019—2023. National Health Interview Survey. . Accessed on: October 28, 2024. https://wwwn.cdc.gov/NHISDataQueryTool/SHS_child/index.html
2. Srinath S, Jacob P, Sharma E, et al. Clinical Practice Guidelines for Assessment of Children and Adolescents. Indian J Psychiatry. 2019;61:158-75. DOI:10.4103/psychiatry.IndianJPsychiatry_580_18
3. Stephan LM. Assessment of Growth and Vital Signs. Pediatric Physical Examination-E-Book: Pediatric Physical Examination-E-Book. 2023:10.

4. Engel JK. Mosby's Pocket Guide to Pediatric Assessment: Elsevier Health Sciences; 2006.
5. Espinoza J, Shah P, Nagendra G, et al. Pediatric Medical Device Development and Regulation: Current State, Barriers, and Opportunities. Pediatrics. 2022;149. DOI:10.1542/peds.2021-053390
6. Rostsinskaja A, Saard M, Sepp K, et al. Characteristics of Pediatric Hospital Fear and Efficiency of New Distraction Technique Holographic Display for Reducing Fear and Pain in Children. Techniques in Neurosurgery & Neurology. 2022;5.
7. Inan OT, Migeotte P-F, Park K-S, et al. Ballistocardiography and seismocardiography: A review of recent advances. IEEE journal of biomedical and health informatics. 2014;19:1414-27.
8. Wei Q, Wang Y, Zhou Z, et al. Classification of Heart Failure Based on Phase Trajectory Complexity of Seismocardiogram. IEEE Sensors Journal. 2023.
9. Erin E and Semiz B. Spectral Analysis of Cardiogenic Vibrations to Distinguish Between Valvular Heart Diseases. BIOSIGNALS; 2023. p. 212-9.
10. Ganti VG, Gazi AH, An S, et al. Wearable seismocardiography-based assessment of stroke volume in congenital heart disease. Journal of the American Heart Association. 2022;11:e026067.
11. Sieciński S, Tkacz EJ and Kostka PS. Heart rate variability analysis on electrocardiograms, seismocardiograms and gyrocardiograms of healthy volunteers and patients with valvular heart diseases. Sensors. 2023;23:2152.
12. Liu L, Yu D, Lu H, et al. Camera-Based Seismocardiogram for Heart Rate Variability Monitoring. IEEE Journal of Biomedical and Health Informatics. 2024.
13. Sang B, Shokouhmand A, Wen H, et al. Identification of S2 paradoxical splitting in aortic stenosis subjects via seismocardiogram signals from a wearable accelerometer contact microphone. IEEE Sensors Journal. 2023;23:15424-34.
14. Nwibor C, Haxha S, Ali MM, et al. Remote health monitoring system for the estimation of blood pressure, heart rate, and blood oxygen saturation level. IEEE Sensors Journal. 2023;23:5401-11.
15. Karimpour P, May JM and Kyriacou PA. Photoplethysmography for the Assessment of Arterial Stiffness. Sensors. 2023;23:9882.
16. Chen Y, Yang X, Song R, et al. Predicting arterial stiffness from single-channel photoplethysmography signal: a feature interaction-based approach. IEEE Journal of Biomedical and Health Informatics. 2024.
17. Linh VTN, Han S, Koh E, et al. Advances in Wearable Electronics for Monitoring Human Organs: Bridging External and Internal Health Assessments. Biomaterials. 2024:122865.
18. Hayirlioglu YZ and Semiz B. PhysioPatch: A Multi-modal and Adaptable Wearable Patch for Cardiovascular and Cardiopulmonary Assessment. IEEE Sensors Journal. 2024.
19. Shandhi MMH, Semiz B, Hersek S, et al. Performance analysis of gyroscope and accelerometer sensors for seismocardiography-based wearable pre-ejection period estimation. IEEE journal of biomedical and health informatics. 2019;23:2365-74.
20. Carek AM, Conant J, Joshi A, et al. SeismoWatch: wearable cuffless blood pressure monitoring using pulse transit time. Proceedings of the ACM on interactive, mobile, wearable and ubiquitous technologies. 2017;1:1-16.
21. Morillo DS, Ojeda JLR, Foix LFC, et al. An accelerometer-based device for sleep apnea screening. IEEE transactions on information technology in biomedicine. 2009;14:491-9.
22. Kaiser JF. On a simple algorithm to calculate the'energy'of a signal. International conference on acoustics, speech, and signal processing: IEEE; 1990. p. 381-4.
23. Semiz B, Hersek S, Whittingslow DC, et al. Change point detection in knee acoustic emissions using the teager operator: A preliminary study in patients with juvenile idiopathic arthritis. 2019 IEEE EMBS International Conference on Biomedical & Health Informatics (BHI): IEEE; 2019. p. 1-4.
24. Semiz B, Carek AM, Johnson JC, et al. Non-invasive wearable patch utilizing seismocardiography for peri-operative use in surgical patients. IEEE journal of biomedical and health informatics. 2020;25:1572-82.
25. Centracchio J, Parlato S, Esposito D, et al. ECG-free heartbeat detection in seismocardiography signals via template matching. Sensors. 2023;23:4684.
26. Lin Y-D and Jhou Y-F. Estimation of heart rate and respiratory rate from the seismocardiogram under resting state. Biomedical Signal Processing and Control. 2020;57:101779.
27. Tokmak F and Semiz B. Investigating the Effect of Body Composition Differences on Seismocardiogram Characteristics. 2023 IEEE 36th International Symposium on Computer-Based Medical Systems (CBMS): IEEE; 2023. p. 323-8.
28. Hughes D, Babbs CF, Geddes L, et al. Measurements of Young's modulus of elasticity of the canine aorta with ultrasound. Ultrasonic imaging. 1979;1:356-67.
29. Payne R, Symeonides C, Webb D, et al. Pulse transit time measured from the ECG: an unreliable marker of beat-to-beat blood pressure. Journal of Applied Physiology. 2006;100:136-41.
30. Yang C and Tavassolian N. Pulse transit time measurement using seismocardiogram, photoplethysmogram, and acoustic recordings: Evaluation and comparison. IEEE journal of biomedical and health informatics. 2017;22:733-40.